FRAGILITY CURVES FOR THE RAPID POSTEARTHQUAKE SAFETY EVALUATION OF BRIDGES

Roy A. Imbsen[1], Shah Vahdani[2], M. Saiid Saiidi[3], Hassan Sedarat[1], and Farid Nobari[1]

[1]SC Solutions, Inc. Sunnyvale
[2]Applied GeoDynamics, Inc., El Cerrito
[3] Infrastructure Innovation, LLC, Reno

Abstract

A new procedure for rapid post-earthquake safety evaluation of bridges has been developed, using existing strong motion records, fragility curves and ground motion data immediately available following an earthquake that will provide the engineer or person directly in charge of the bridge to make a more informed decision to close or keep a bridge open to traffic. The recently constructed Carquinez I80 West Bridge (Alfred Zampa Memorial Bridge) was selected to demonstrate the procedure. This paper describes the detailed time history finite element analysis conducted using strong motion data for the 26 scenario earthquake events and the development of the fragility curves using shake table test results on reinforced concrete columns tested through five damage states to final failure. Fragility functions are developed for various seismic parameters for each damage state and calibrated for maximum drift ratios for inclusion into the rapid safety evaluation of the Carquinez Bridge.

Introduction

This study, entitled *Rapid Post-Earthquake Safety Evaluation of the New Carquinez Bridge Using Fragility Curves and Recorded Strong-Motion Data* is part of the Data Interpretation Project of the California Strong Motion Instrumentation Program (CSMIP) in the Department of Conservation (DOC) California Geological Survey. The purpose of this project is to accelerate the application of the strong-motion data in reducing risk due to the strong earthquake shaking which occurs in California.

Overview of the Safety Evaluation Procedure

The application of the procedure undertaken in this study is to provide for the selected New Carquinez Bridge, as shown in Figure 1, the ability to assess the damage immediately following an earthquake using the ground motion parameters of the earthquake event and fragility curves developed for the bridge so that a decision can be made on the continued use or closure of the bridge.

Figure 1: Aerial View of the New Carquinez Bridge

Background

SC Solutions (SCS) was tasked to develop a system to improve the current Caltrans rapid post-earthquake decision making process for critical bridges. Immediately after any earthquake, Caltrans has to make decisions about the post-earthquake conditions of bridges. The decision making process will be based on the magnitude of the earthquake event, location of a bridge, instrument data, the understanding of the performance of the bridge in the subject earthquake, and factors related to risk and consequences. Most of the critical bridges that are in high seismic zones are instrumented. These instrument data are monitored in real time and can be used for this decision making process. The foundation or free field ground motions near the bridge and some of the structural performance can be obtained immediately after an earthquake. However, this limited instrument data doesn't provide adequate information about the conditions of all critical components of bridges immediately after an event. Therefore, additional understanding of the bridge performance and fragility functions should be developed for each of these critical bridges to assist the post-earthquake decision making process.

To develop fragility functions, first a set of pre-earthquake scenario events must be selected based on the location of the bridge and the active faults in the vicinity of the bridge site. For this task SC Solution proposed to use the New Carquinez Bridge for the case study. After selecting a set of scenario earthquakes for the New Carquinez Bridge, the existing SCS bridge model could be used to simulate the effects of these ground motions to understand the performance of each critical component in the bridge. After conducting these pre-earthquake seismic analyses, a relationship can be developed between the earthquake intensity parameter (e.g. magnitude, distance and spectral acceleration) and the primary response parameter of a critical component.

As one example, the primary response parameter can be a drift for a critical tower. Based on the primary response parameter value, a damage index (or damage potential) can be developed for each critical component. This damage potential can be related to the seismic intensity parameter as a fragility function for each critical component.

Pre-Event Data Processing

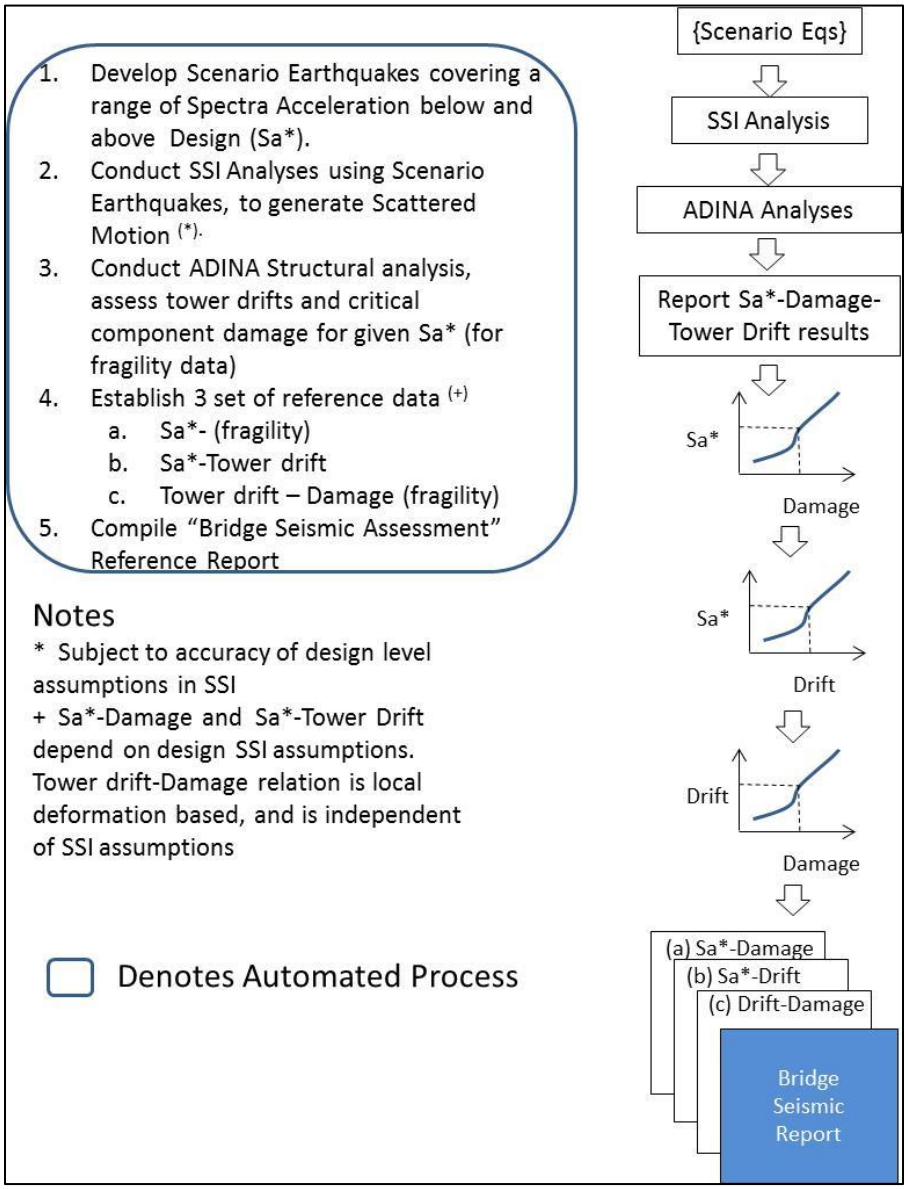

Figure 2: Pre-Event Data Processing

As shown in Figure 2, prior to an event, several automated procedures will be completed and compiled in a "Bridge Seismic Assessment" report, as a reference document for Caltrans decision making, after an event. The steps include the following:

a. Establish Scenario Earthquakes

To develop fragility functions, a set of pre-earthquake scenario events must be selected based on the location of the bridge and the active faults in the vicinity of the bridge site. For the purpose of this project, 26 sets of scenario ground motions were generated based on different

magnitude earthquakes on regional faults. These motions ranged from low fault activity and spectral acceleration, through Design Spectra, and spectral acceleration values both less than and greater than design levels prescribed for the site. The characteristics of each motion were identified by moment magnitude (Mw), distance to the fault (R), and spectral acceleration (Sa).

b. Develop Input Ground Motions at the Bridge Site

Using the available site specific ground motion, generation tools and design spectra, the SSI analytical model customized for the Carquinez site was used to bring the scenario earthquakes to the site and to generate scattered motions.

c. Dynamic Analyses of Bridge under Scenario Ground Motions (Demand)

The existing detailed Finite Element model of the New Carquinez Bridge [13, 21, 29], developed by SCS, was used in the demand analyses subjected to the scenario ground motions. Drift values of the critical components of the bridge were related to the motion characteristics (Mw, R, Sa). For each critical component, a primary response parameter should be identified. In this project, the proposed approach and scope-of-work is demonstrated for Tower 3 drift as the primary response parameter to reflect the damage state of Critical Tower Components, as an example of the process. This methodology can be applied to different primary response parameters to reflect damage status of other critical components.

d. Pushover Analysis (Capacity)

A Finite Element model of Tower 3 was used to perform pushover analysis. Values of drift and strain (concrete and reinforcement) were extracted and correlated.

e. Evaluation of Tower Drift and Component Damage (relationship between demand and capacity)

Governing tower drifts as the primary response parameters were documented vs. motion characteristics (Mw, R, and Sa), and finally a series of relationships between the motion characteristics (Mw, R, and Sa), Tower Drift, and strain values (damage) of the critical tower were generated.

f. Develop Fragility Data versus Earthquake Intensity and Tower Drift

Based on the analyses, the following response parameters were related to the scenario earthquake intensity, fault, and distance to site:

- Relation between damage states (DS) and strain (Fragility),
- Relation between strain and drift (pushover analysis)
- Using the above, obtain Relation between damage state (DS) and drift (Fragility),
- Relation between (Mw, R, Sa) and drift (26 time-history analyses)

Description of the New Carquinez Bridge and Local Seismic Design Hazard

Description

The New Carquinez Bridge spans the Carquinez Strait with a 2,388 ft. main span bounded by a south span (towards Oakland) of 482 ft. and a north span (towards Sacramento) of 594 ft. as shown in Figure **3**. The principal components of this suspension bridge include

reinforced concrete towers supported on large-diameter concrete pile foundations, parallel-wire cables, gravity anchorages, and a closed orthotropic steel box deck system. The main concrete towers are approximately 400 ft. tall, and are tied together with a strut below the deck and upper strut between the cable saddles as shown in the Typical Section view included in Figure **3**. The lower strut supports the deck vertically using two rocker links and transversely through a shear key.

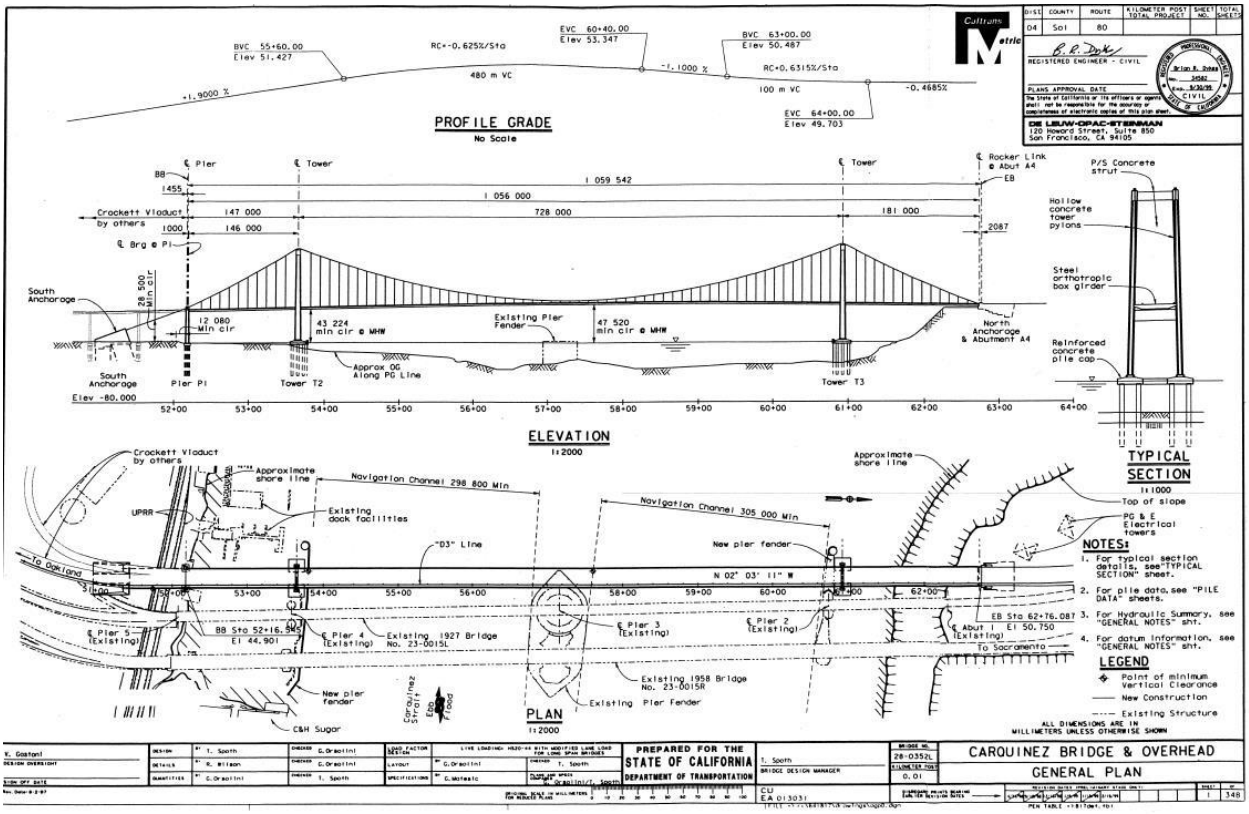

Figure 3: General Plan

Local Seismic Design Hazard

The bridge site, located approximately twenty miles northeast of San Francisco, is located in an active seismic zone. Seismic hazard assessments have shown that the site could be subject to strong ground motions originating on the San Andreas Fault, the Hayward Fault, Concord-Green Valley Fault, Napa Valley Fault, and the Franklin Fault. However, studies have shown that the Hayward fault, Concord-Green Valley fault system, and the Napa Valley seismic zones are the dominant sources of seismic hazard for the bridge's frequency range.

The seismic design of the New Carquinez Bridge considers both the Safety Evaluation Earthquake (SEE) and the lower level Functional Evaluation Earthquake (FEE). Caltrans performance requirements for these events are higher than the minimum level required for all transportation structures but below that required for an Important Bridge. As much as possible, the Important Bridge criteria are to be met for the Safety Evaluation Earthquake (SEE) corresponding to a maximum credible event which has a mean return

period in the range of about 1,000 to 2,000 years. In this earthquake, the bridge can be subject to primarily "minor" damage with some "repairable" damage to piles, pile caps and anchorage blocks and still remain open.

Structural Analysis

A detailed finite element model of the New Carquinez Bridge was developed based on the marked up drawings [10], using the ADINA FE program [31]. All structural components of the new Carquinez Bridge were explicitly modeled. A cross-section of the steel box girders and the bulkhead details are shown in Figure 4. The side elevation view is shown in Figure 5. The key structural components that were included in the global FE model are summarized in Table 1. Suspension bridges belong to a category of bridges that are highly nonlinear in geometry and therefore, during the construction simulation and for their seismic evaluation, large displacement capability was included in the analysis. Geometry iteration was used for the construction sequence of the NCB FE detailed model [7, 22].

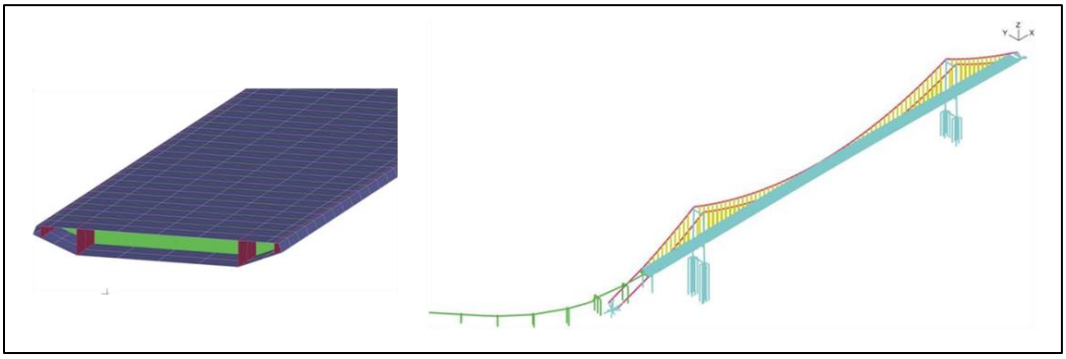

Figure 4: Detailed FE Model of the New Carquinez Bridge (Alfred Zampa Memorial Bridge)

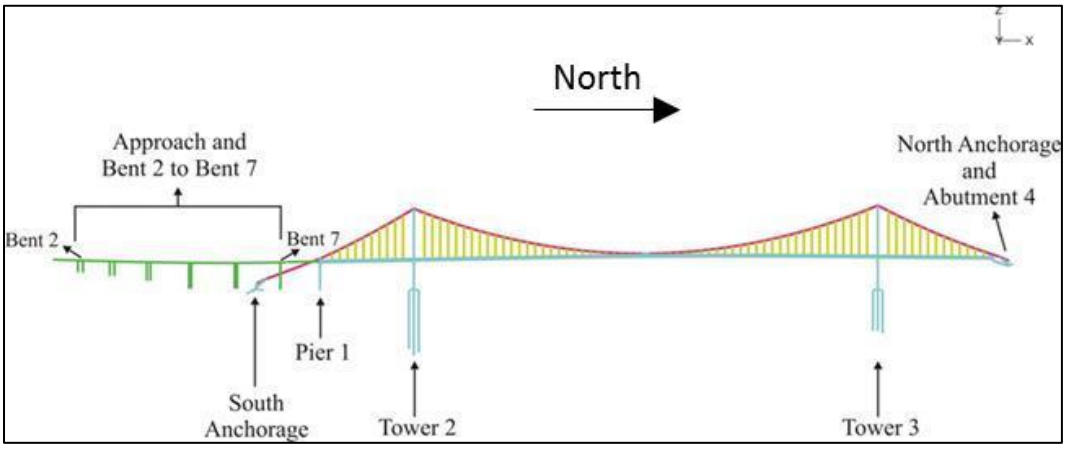

Figure 5: Elevation View of Detailed Model

Pushover Analysis of Tower 3 (Capacity Calculation) - Drift-Strain Curves

The stand-alone FE model of Tower T3 was developed with a fixed base. The pushover profile is proportional to the first longitudinal mode of vibration for the tower, which was obtained from the global model. The main reason to perform pushover analysis is to obtain drift-strain curves (capacity), which will be used as an input to the fragility analysis.

Table 1: Key Structural Components [29]

Component	Description / Model
Main Cables	37-strand cables with 232-wires per strand Linear elastic beam elements with (partially non-composite moment of inertia)
Hangers (suspenders)	four galvanized structural steel ropes Linear elastic truss elements
Towers	Reinforced concrete box section Localized plasticity at the location of plastic hinges ADINA moment-curvature beam elements
Superstructure	Orthotropic steel deck 8-noded shell elements with orthotropic properties
Rocker Links	Steel rocker Beam elements
Anchorages at the North and South sides	Reinforced concrete Rigid links
Piles	Reinforced concrete Moment-curvature beam elements
SSI modeling at piles	PY Nonlinear plastic truss elements TZ and QZ Nonlinear elastic spring elements
SSI modeling at anchorages	Soil impedance General elements: Stiffness, damping and mass matrices

Force-Displacement Curves from Pushover Analysis

The pushover analysis of Tower T3 was performed using the first longitudinal mode of the tower. The inflection point location varies as the push forces increase. The force-displacement of the tower is shown in Figure 6. The values of strain in confined concrete and steel are also shown in this figure. The steel and concrete strain values along with the location of the point of inflection are summarized in Table 2. The steel and concrete strain limits, based on the design criteria [6] are 0.012, and 0.06 for concrete and steel, respectively. The steel strain reached its limit, before the concrete, and at about a 6-ft displacement at the top of the tower. The maximum relative top-to-bottom displacement of tower T3 from the PS&E analysis is 1.45-ft [8].

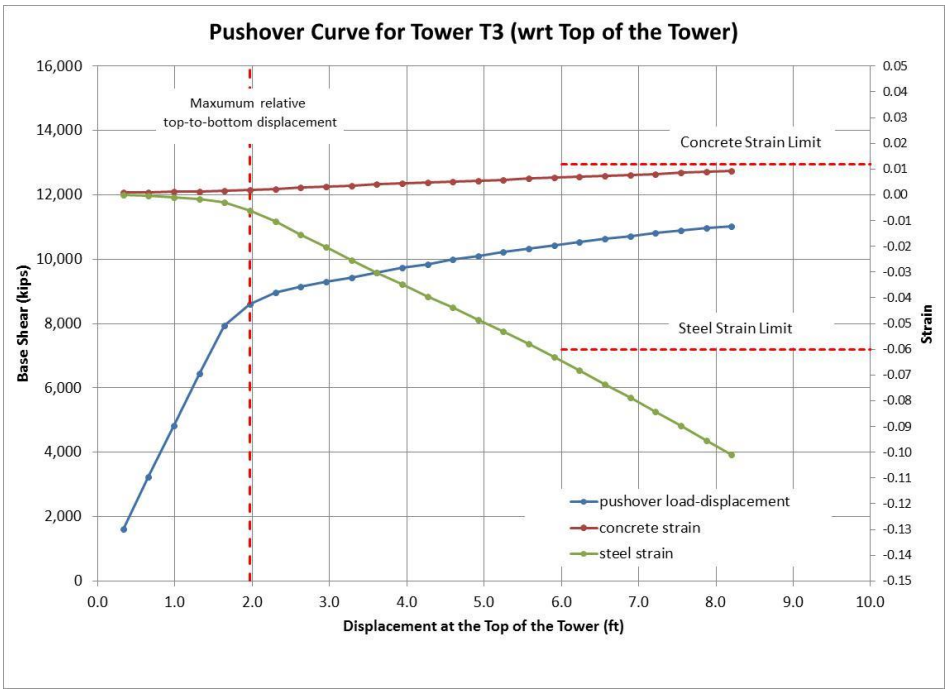

Figure 6: Total Base Shear - Displacement Relationships of Tower T3

Nonlinear Dynamic Analyses of the Detailed Model of the NCB – (Mw, R)-Strain Relation

In order to obtain a relationship between ground motion characteristics (Mw, R) and damage (from fragility analysis), the relationship between the ground motion characteristics (Mw, R) and the strain in concrete and steel should be obtained first. The relationship between the capacity drift and strain was obtained from the pushover analysis. In this study, the demand values which are the relationship between the ground motion characteristics (Mw, R) and drift has been obtained from 26 nonlinear time-history analyses for the 26 scenario ground motions. The relationship between the ground motion characteristics (Mw, R) and strain can be obtained by combining the results obtained from the pushover analysis and time-history analyses, as described Table 3 and Figure 7**.**

Table 2: Force-Displacement-Strain Relationships of Tower T3

step	relative displacement (ft) lower strut to base Δ	relative displacement (ft) upper strut to base Δ	PI (ft)	base shear (kip)	strains at base	
1.01	0.15	0.33	112.32	1.61E+03	6.18E-05	9.06E-04
1.02	0.30	0.66	112.32	3.23E+03	-4.80E-04	1.10E-03
1.03	0.44	0.98	112.32	4.83E+03	-1.06E-03	1.25E-03
1.04	0.59	1.31	112.32	6.44E+03	-1.66E-03	1.39E-03
1.05	0.74	1.64	112.22	7.93E+03	-2.89E-03	1.60E-03
1.06	0.89	1.97	111.35	8.61E+03	-6.09E-03	1.98E-03
1.07	1.03	2.30	110.17	8.96E+03	-1.04E-02	2.35E-03
1.08	1.18	2.62	108.89	9.15E+03	-1.54E-02	2.76E-03
1.09	1.33	2.95	107.64	9.31E+03	-2.04E-02	3.22E-03
1.1	1.48	3.28	106.42	9.44E+03	-2.54E-02	3.69E-03
1.11	1.62	3.61	105.23	9.58E+03	-3.02E-02	4.12E-03
1.12	1.77	3.94	104.08	9.73E+03	-3.48E-02	4.50E-03
1.13	1.92	4.27	102.97	9.85E+03	-3.94E-02	4.88E-03
1.14	2.07	4.59	101.88	9.99E+03	-4.38E-02	5.23E-03
1.15	2.21	4.92	100.82	1.01E+04	-4.84E-02	5.57E-03
1.16	2.36	5.25	99.79	1.02E+04	-5.29E-02	5.91E-03
1.17	2.51	5.58	98.79	1.03E+04	-5.79E-02	6.28E-03
1.18	2.66	5.91	97.80	1.04E+04	-6.29E-02	6.66E-03
1.19	2.81	6.23	96.84	1.05E+04	-6.81E-02	7.04E-03
1.2	2.95	6.56	95.90	1.06E+04	-7.35E-02	7.41E-03
1.21	3.10	6.89	94.98	1.07E+04	-7.88E-02	7.79E-03
1.22	3.25	7.22	94.07	1.08E+04	-8.42E-02	8.17E-03
1.23	3.40	7.55	93.18	1.09E+04	-8.97E-02	8.56E-03
1.24	3.54	7.87	92.28	1.10E+04	-9.53E-02	8.96E-03
1.25	3.69	8.20	91.40	1.10E+04	-1.01E-01	9.35E-03

Table 3: Ground Motion (M/R) – Relative Drift at the Top of Tower and at PI – Strain in Steel and Concrete at the Base of the Tower

North-West Leg						combine Pushover - TH		strain at the base	
						Relative Drift @ Top	Relative Drift @ PI		
GM run ID	Scenario	RSN	Ground Motion Name	M	R (km)	(ft)	(ft)	steel	concrete
1	1	1176	1999 Kocaeli Turkey	7.51	1.38	1.31	0.39	-1.655E-03	1.387E-03
2	3	1244	1999 Chi-Chi Taiwan	7.62	9.94	1.43	0.43	-2.086E-03	1.461E-03
3	16	8099	2011 Christchurch New Zealand	6.2	17.86	0.40	0.12	-5.989E-05	9.496E-04
4	17	4078	2004 Parkfield-02 CA	6	22.45	0.33	0.10	6.180E-05	9.063E-04
5	21	1120	1995 Kobe Japan	6.9	1.46	1.48	0.44	-2.289E-03	1.496E-03
6	22	159	1979 Imperial Valley-06	6.53	0.00	1.19	0.36	-1.438E-03	1.338E-03
7	2	292a	1980 Irpinia Italy-01	6.9	6.78	0.95	0.28	-9.954E-04	1.236E-03
8	4	864	1992 Landers	7.28	11.03	1.08	0.32	-1.234E-03	1.292E-03
9	5	5831	2010 El Mayor-Cucapah Mexico	7.2	14.80	0.76	0.23	-6.635E-04	1.148E-03
10	6	1045 a	1994 Northridge-01	6.69	2.11	0.72	0.22	-5.949E-04	1.130E-03
11	7	1114	1995 Kobe Japan	6.9	3.31	1.14	0.34	-1.345E-03	1.317E-03
12	8	161	1979 Imperial Valley-06	6.53	8.54	0.73	0.22	-5.893E-04	1.147E-03
13	9	4847	2007 Chuetsu-oki Japan	6.8	9.43	0.90	0.27	-9.113E-04	1.213E-03
14	10	6961	2010 Darfield New Zealand	7	13.37	0.62	0.19	-4.251E-04	1.080E-03
15	11	6923	2010 Darfield New Zealand	7	30.53	0.50	0.15	-2.145E-04	1.005E-03
16	12	292b	1980 Irpinia Italy-01	6.9	6.78	0.63	0.19	-4.111E-04	1.107E-03
17	13	8123	2011 Christchurch New Zealand	6.2	5.11	0.79	0.24	-7.121E-04	1.161E-03
18	14	1045 b	1994 Northridge-01	6.69	2.11	0.55	0.16	-3.030E-04	1.036E-03
19	15	313a	1981 Corinth Greece	6.6	10.27	0.49	0.15	-2.109E-04	1.003E-03
20	18	569	1986 San Salvador	5.8	3.71	0.43	0.13	-1.128E-04	9.685E-04
21	19	147	1979 Coyote Lake	5.74	8.47	0.47	0.14	-1.742E-04	9.903E-04
22	20	149	1979 Coyote Lake	5.74	4.79	0.45	0.13	-1.330E-04	9.757E-04
23	23	1054	1994 Northridge-01	6.69	5.54	1.31	0.39	-1.662E-03	1.388E-03
24	24	1236	1999 Chi-Chi Taiwan	7.62	37.48	0.81	0.24	-7.528E-04	1.171E-03
25	25	2111	2002 Denali Alaska	7.9	42.99	0.38	0.11	-2.552E-05	9.374E-04
26	26	313b	1981 Corinth Greece	6.6	10.27	0.55	0.16	-3.025E-04	1.036E-03

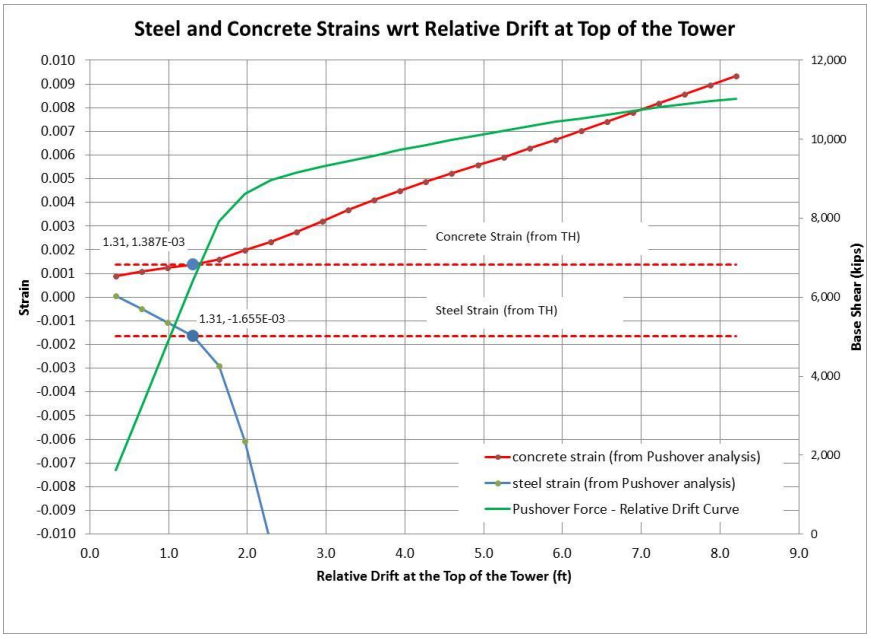

Figure 7: Drift and Strain in Concrete and Steel using TH Analysis and Pushover Curves (Run ID1: 1999 Kocaeli Turkey -- Typical)

Development of Fragility Relationships

This section presents a summary of the work on development of fragility relationships for the Carquinez Bridge east tower subjected to earthquakes in the longitudinal direction of the bridge. The purpose of the curves is to provide a probabilistic estimate of damage states as a function of the maximum drift ratio, which is relatable to the spectral acceleration (S_a), the moment magnitude (M_w) and the distance to the site (D), expressed as $S_a(M_w, D)$.

Experimental Database

The objective of this step was to develop fragility curves for the Carquinez Bridge Tower 3 (T3) using experimental database [20] obtained at the University of Nevada, Reno (UNR), and analytical ADINA response data. More than 100 shake table test data from studies of over 20 reinforced concrete (RC) bridge column models conducted at the University of Nevada, Reno (UNR) was used. The test columns were designed based on recent or current seismic design provisions used at Caltrans [20].

Definition of Damage States

Six apparent damage states (DS) were developed for RC columns in cooperation with Caltrans engineers involved in the reconnaissance investigations [20]. These damage states were correlated with different seismic response parameters. The apparent damage states and the corresponding maximum longitudinal bar strains (MLS) were used respectively as limit states and the response parameter. The damage states (see Figure 8 to Figure 10) are defined as:

- DS-1: Flexural cracks;
- DS-2: Minor spalling and possible shear cracks;
- DS-3: Extensive cracks and spalling;
- DS-4: Visible lateral and/or longitudinal reinforcing bars;
- DS-5: Compressive failure of the concrete core edge (imminent failure); and
- DS-6: Failure.

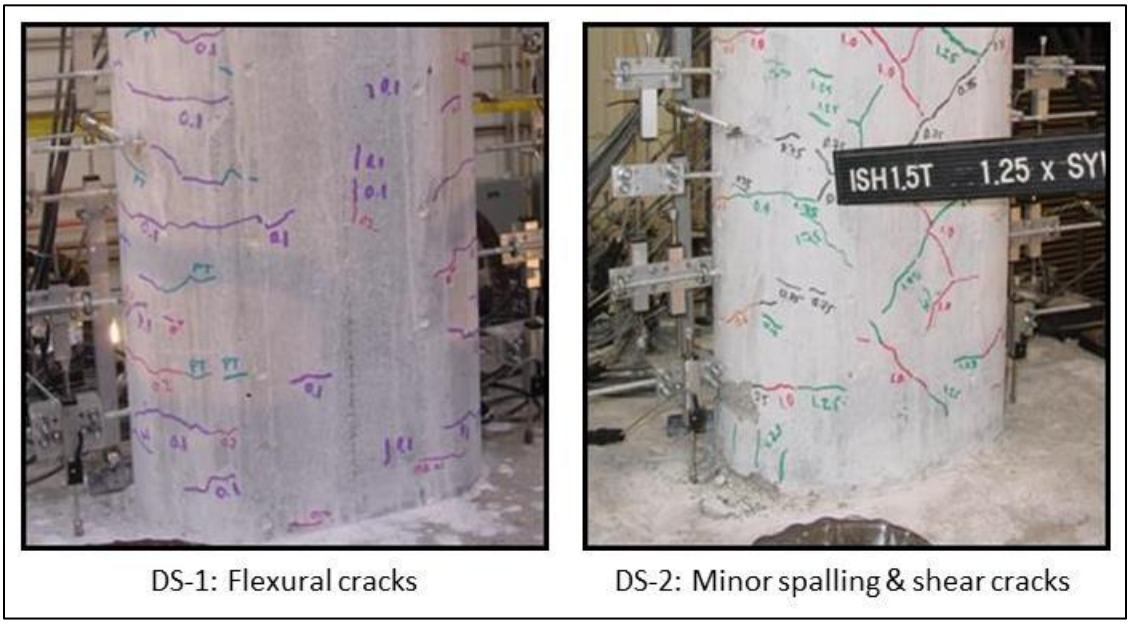

Figure 8: Damage States 1 and 2 - Apparent damage states in the RC bridge columns [20]

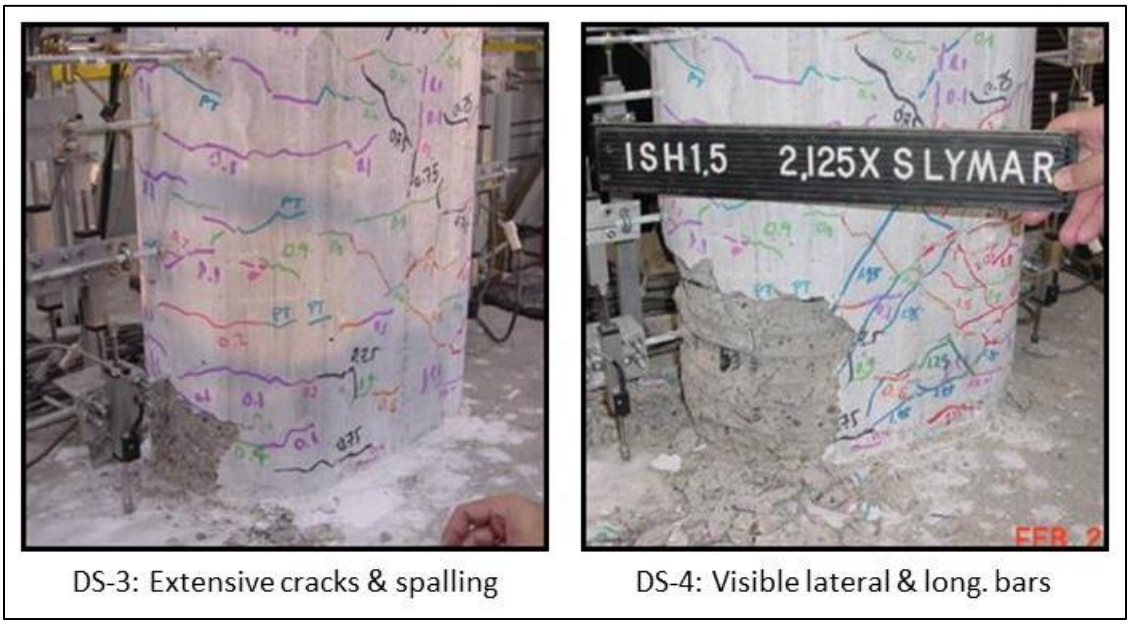

Figure 9: Damage States 3 and 4 - Apparent damage states in the RC bridge columns [20]

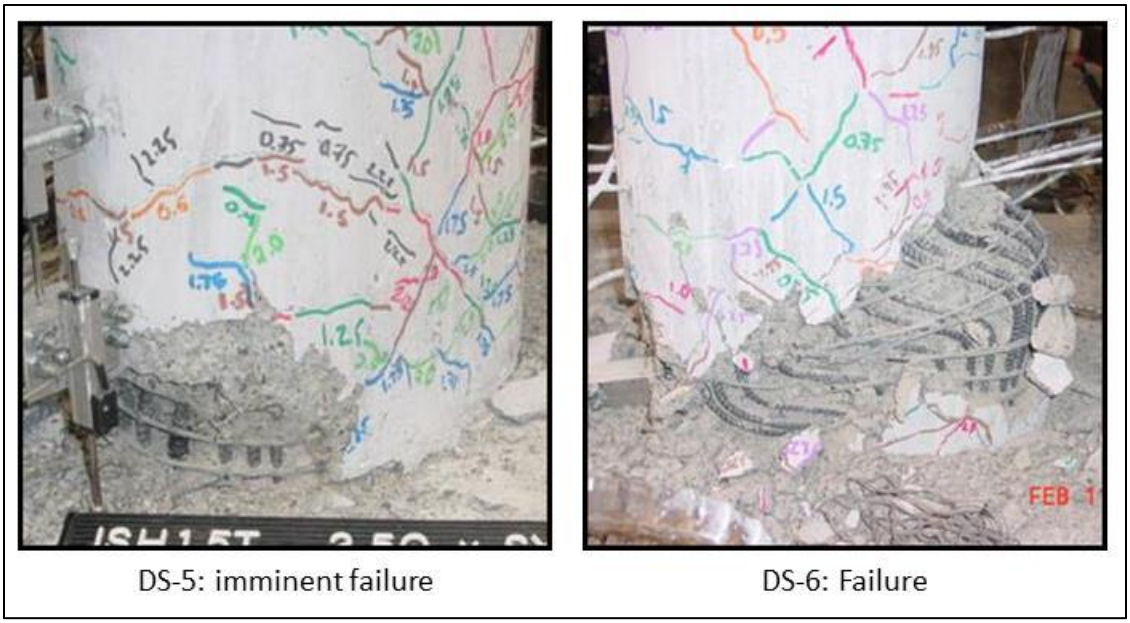

Figure 10: Damage States 5 and 6 - Apparent damage states in the RC bridge columns [20]

Lognormal cumulative distribution function was used to correlate damage states to response parameters. The correlation between the first 5 damage states and MLS is presented in Figure 11.

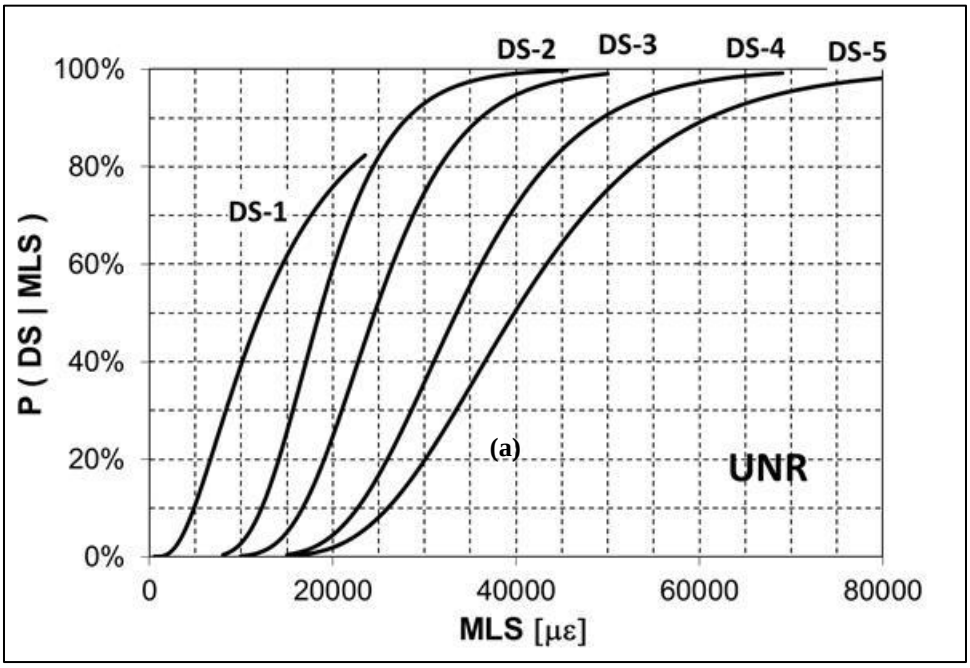

Figure 11: MLS Fragility Curves for UNR Shake Table Database

Calibration of Experimental Fragility Curves for Tower T-3

The column test models mostly had circular sections. A method was developed to calibrate the measured MLS fragility curves for the hollow section of Tower T-3. Steel and concrete strains were used as indicators of the damage states. Flexural cracks are formed on the tensile side of an RC member. Therefore, MLS is a reasonable indicator for DS-1 and consequently the measured MLS fragility curve for DS-1 was used directly for T-3. Apparent DS-2 to DS-5 are due to damage in concrete on the compressive side. Therefore, the maximum compressive strain in concrete was viewed as an indicator of these damage states. Since the experimental database is based on MLS for all damage states, a calibration factor was developed for MLS at DS-2 to DS-5 assuming that the extreme compression fiber strains in T-3 are the same as those in the circular columns of the experimental database. If the ratio of concrete to steel strain in the extreme fibers of circular columns is α and that of T-3 is β, the calibration factor for DS-2 to DS-5 (Figure 12) is α/β.

- α is the ratio of concrete to steel strain in the extreme fibers of circular columns, and
- β is the ratio of concrete to steel strain in the extreme fibers of T3

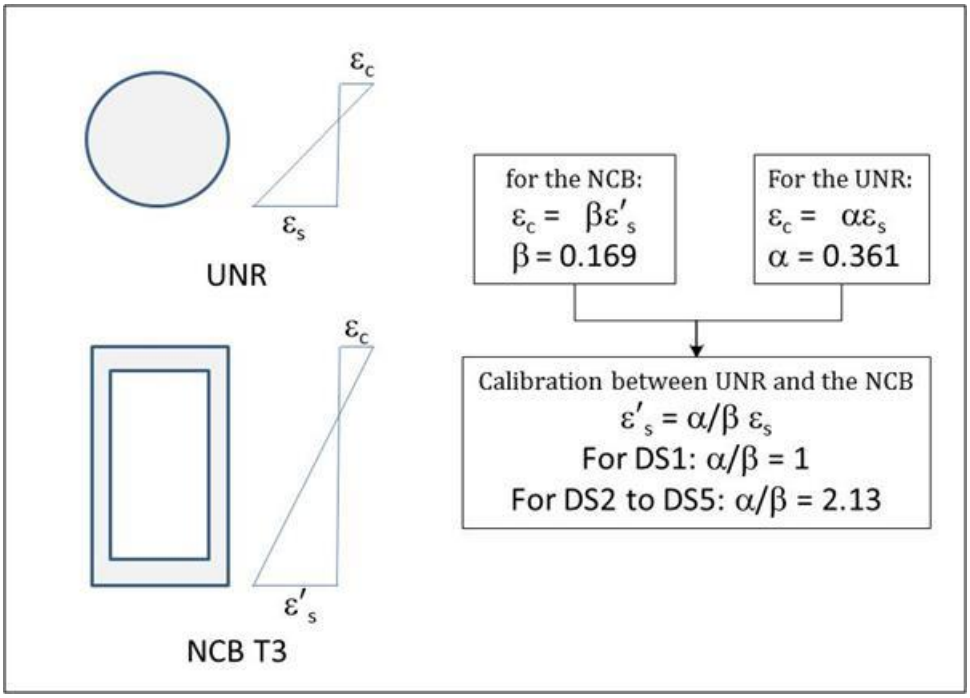

Figure 12: Schematic of Strain Ratios used for Calibration Procedure (for DS-2 to DS-5)

Figure 13 illustrates the strain diagram in a circular RC column. In this figure, ε_c and ε_s are extreme fiber strains in concrete and steel, respectively, ε_t is extreme tensile fiber strain, c is the compression depth, and D is diameter of the circular column. It can be assumed that ε_s and ε_t are approximately the same. Therefore, α was calculated as 0.361 using the following equation:

$$\alpha = \frac{\varepsilon_c}{\varepsilon_s} = \frac{1}{\frac{1}{c/D} - 1} \tag{1}$$

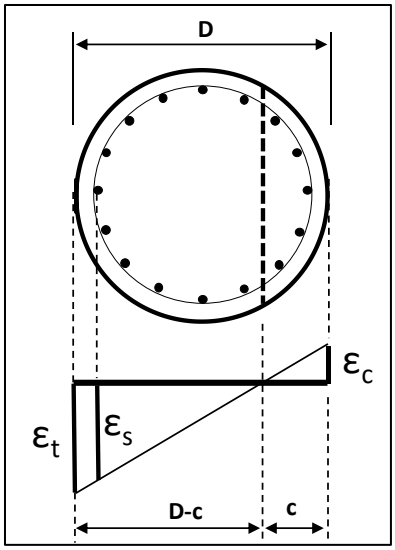

Figure 13: Strain diagram in a circular RC column

The c/D ratio for circular columns was calculated using the following equation [35]:

$$c / D = 0.2 + 0.65 \frac{P}{f'_{ce} A_g} \tag{2}$$

Where P is axial force, f'_{ce} is concrete expected strength, and A_g is the gross section area of the circular column. β was calculated as 0.169 (see Figure 12) based on the strain data listed in Table 3 at the maximum compressive concrete strain of 0.003. The resulting calibration factor (α/β) was 2.13 (see Figure 12).

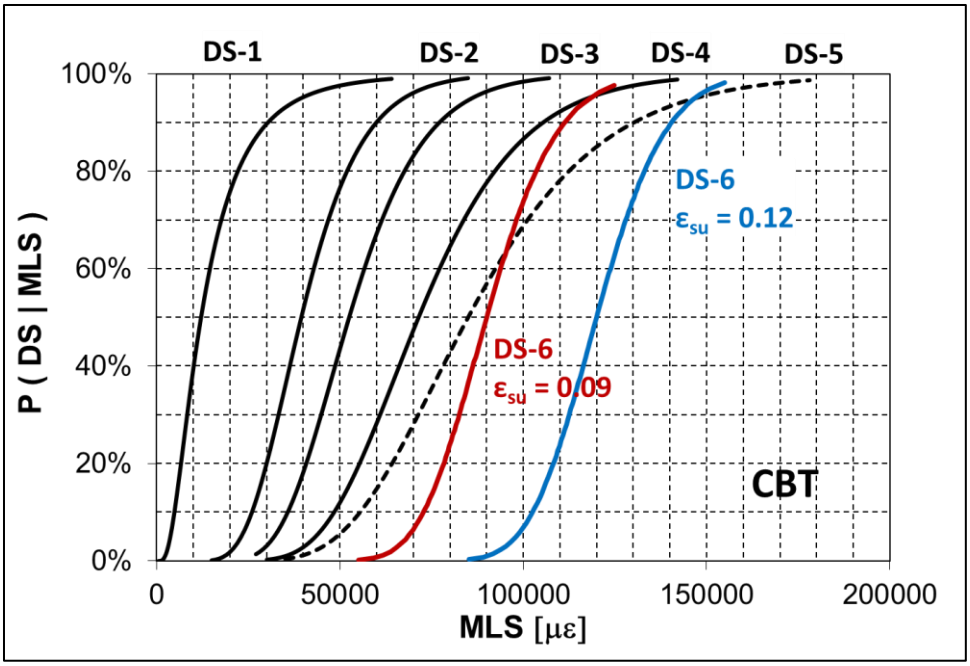

Figure 14: Calibrated maximum longitudinal bar strains (MLS) fragility curves for T-3

Fragility Curves for Tower 3 (T3)

The maximum drift ratio (MDR) fragility curves were developed for T-3 based on the correlation between MLS and MDR. The relationship between MLS and MDR was identified based on strain data and pushover analysis (see Figure 6 and Table 2) after the calculated curve was idealized with a bilinear curve. The relation between maximum drift ratio (MDR) and maximum longitudinal strain (MLS) is shown in Figure 15 . The relation between drift fragility and MDR is shown in Figure 16 . Therefore, knowing MLS, the value of MDR can be estimated (Figure 15**)** Using the value of MDR and (Figure 15**)** the value of fragility can be estimated. The fragility curves (Figure 16) were prepared for six Damage States (DS) and relate the maximum drift ratio (MDR) to the probability of occurrence (POC) for each DS.

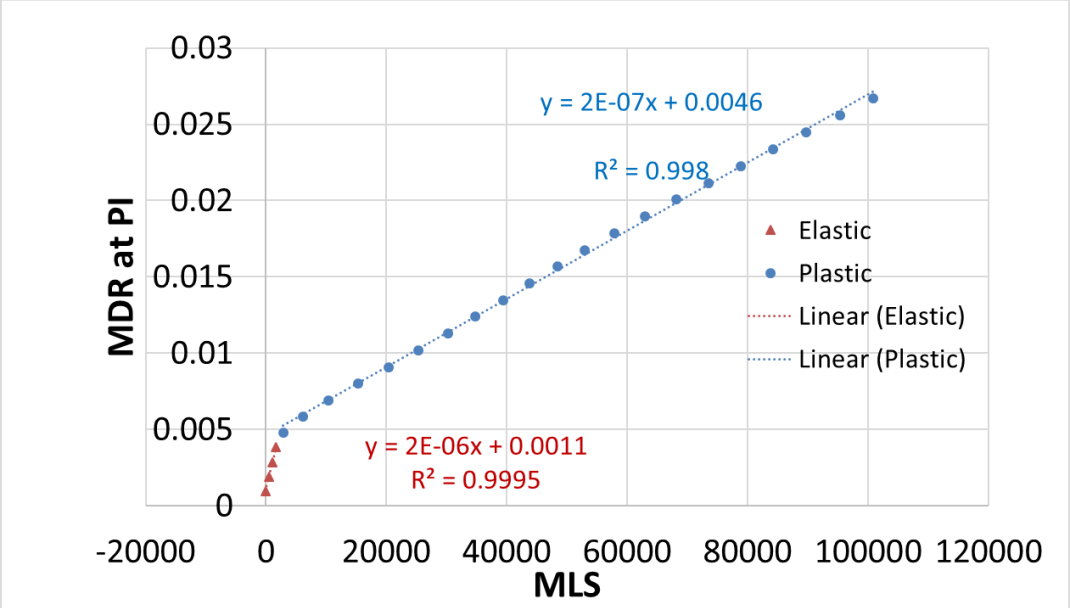

Figure 15: MLS-MDR relationship in T-3 at Inflection Point

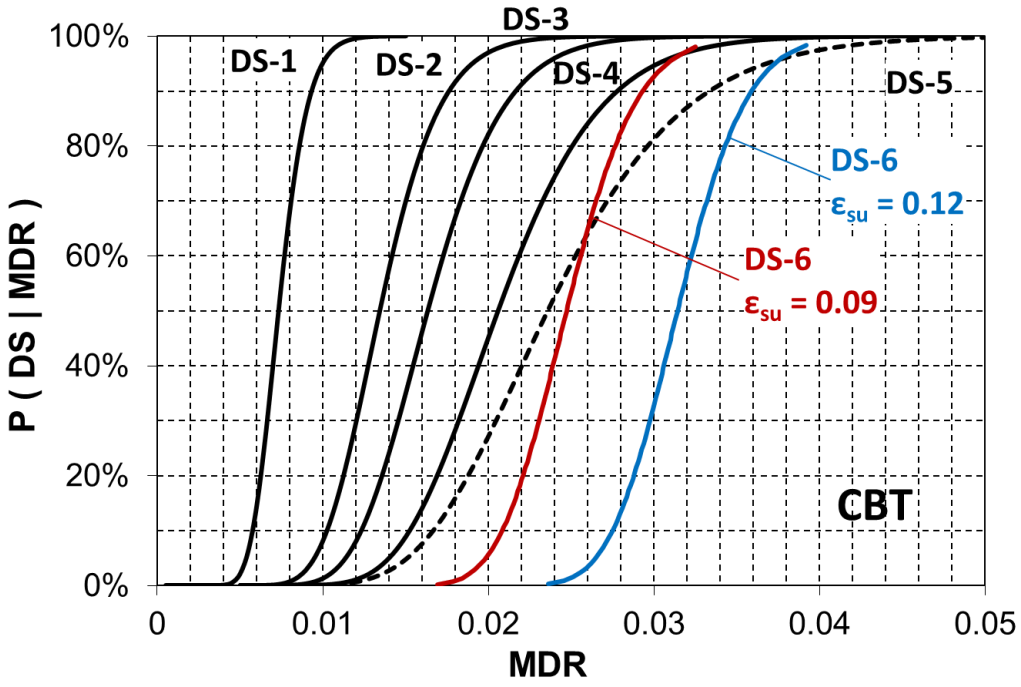

Figure 16: Maximum drift ratio fragility curves for T-3

Application of Proposed Rapid Safety Evaluation Procedure

Immediately after Event

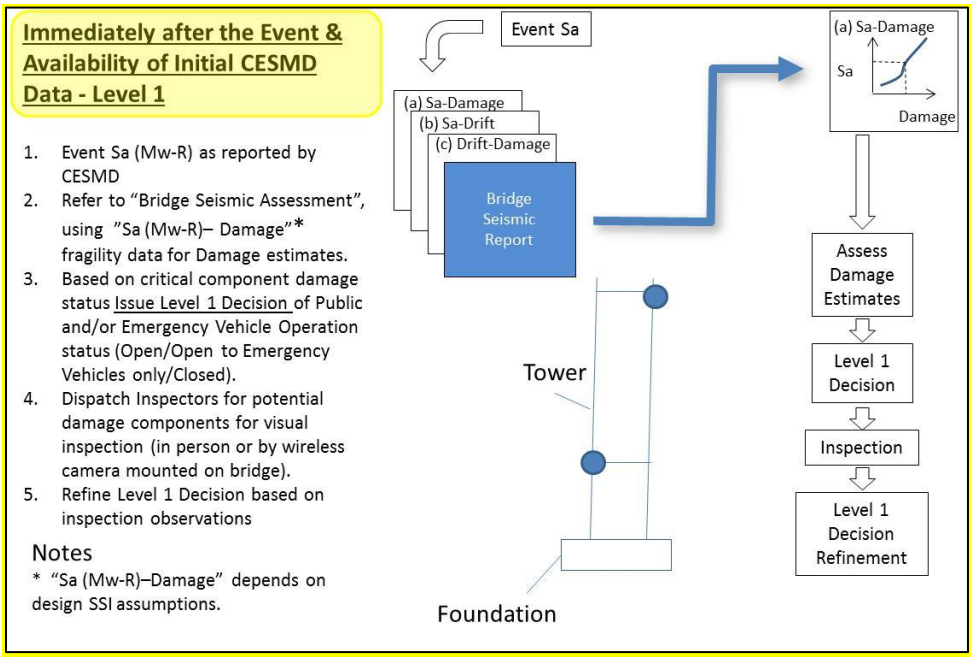

Figure 17: Immediately after Event Data Processing

As shown in Figure 17, immediately after an event, two levels of decisions can be made:

Level 1: this is a quick, but educated, decision making based on the relationship between spectra acceleration and damage.

Level 2: This is a more rigorous evaluation which requires the recoded data, and therefore takes more time. Using the measured drift values, use the fragility curves to estimate potential damage.

The followings are steps to be followed for this stage of data processing:

1. Use Spectra acceleration Sa(Mw-R) versus Damage generated in the pre-event data processing. This is "level 1" decision making based on the potential damage in the bridge.
2. Recover tower drift from CSMIP measured data.
3. Assess damage from the relationship between fragility and drift obtained in step 6 of the pre-event data processing.
4. Using the measured drift values and fragility curves, estimate the potential damage in the bridge. This is "level 2" decision making.
5. Alert inspection crew for anticipated damage and request for confirmation.

Post Event Data Processing

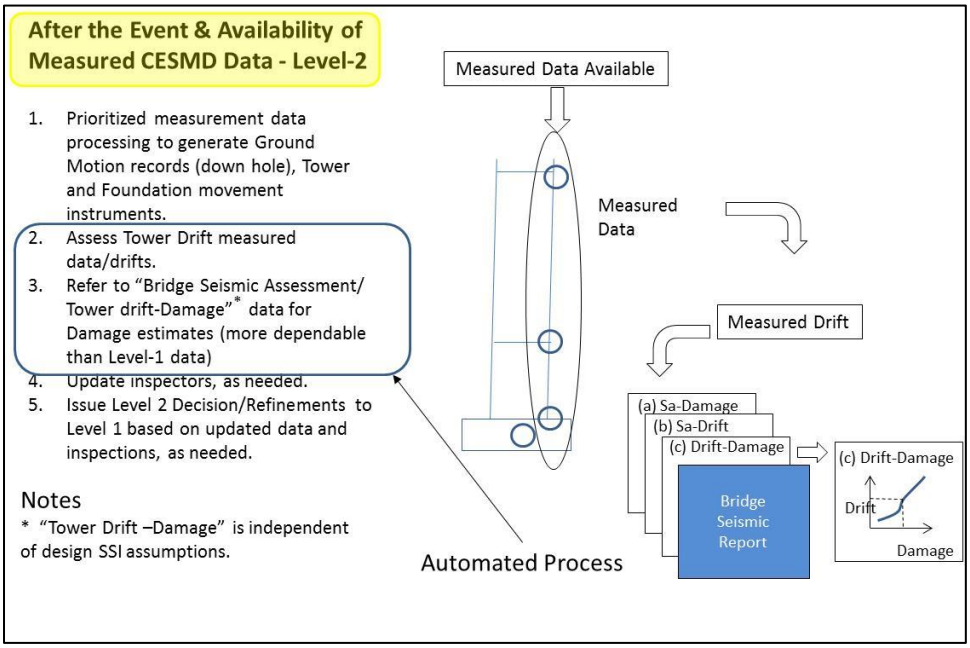

Figure 18: After Event Data Processing

In the "Post Event" data processing (see Figure 18), there is more time to improve on modeling of the structure as well as soil and interaction between the two. Also, the measured data can be studied in more detail. The following steps will be taken in this stage:

1. Compare measured scattered motion at the foundation with the estimated motions that were calculated in "pre-event" step 2.
2. Improve assumptions in the ground motion generation in "pre-event" step 2 based on the differences between the measured and calculated data.
3. Repeat and refine drift and fragility data analysis (steps 1 to 5 of the "pre-event" Figure 2), based on the improved ground motions

Conclusions

In this study, the prototype for a procedure was successfully developed to assess the damage immediately following an earthquake using the ground motion parameters of the earthquake event and fragility curves developed for the bridge so that a decision can be made on the continued use or closure of the bridge. This procedure, in this prototype, was implemented the west tower (T3) of the New Carquinez Bridge. For the 26 scenario ground motions the damage was observed for the longitudinal direction using the MDR and the fragility curves. The following steps were taken to successfully evaluate the damage state for the tower in the longitudinal direction. The scope of the current study is to evaluate seismic performance of Tower T3 in the longitudinal direction as "a critical component" of the bridge. The procedure

that is presented in this report can be equally applied to all other key components of the bridge, to produce system-wide fragility information, and base the bridge serviceability decision on the response of the governing key component.

1. A pushover analysis was performed to obtain the force-strain-drift relation of the tower.
2. The fragility curves for the Carquinez Bridge (NCB) Tower 3 (T3) were developed using experimental database obtained at the University of Nevada, Reno (UNR), and analytical ADINA response data were obtained for the demand. More than 100 shake table test data from studies of over 20 reinforced concrete (RC) bridge column models conducted at the University of Nevada, Reno (UNR) was used. The test data were calibrated for the cross section of the tower leg and the fragility curves for the Tower T3 were developed. The fragility curves (Figure 16, also shown in Figure 19) were prepared for six Damage States (DS) and relate the maximum drift ratio (MDR) to the probability of occurrence (POC) for each DS.
3. Values of MDR were computed and summarized in Table 4 for 26 scenario ground motions, using nonlinear time-history analysis of the detailed 3D model of the NCB. As shown in this table, each scenario has been defined by Mw, R, and Sa as well as the name of the event. Relative drift at the top of the tower T3 and at the location of point of inflection (PI) as well as maximum strain values in concrete and steel are summarized in this table. Therefore, this table provides a database of event (Mw, R, Sa) and MDR for tower T3.
4. For any MDR in this table, and using Figure 19, the fragility can be readily obtained; indicating that for all the 26 scenario cases there will be 0% POC for MS1. This is in conformance with the values of strain in steel and concrete summarized in Table 4.
5. While no damage was detected in the longitudinal Tower direction (i.e. subject of the study), the condition of other key components in a comprehensive system-wide evaluation may result in critical damage states.
6. These steps can be applied to evaluate the performance of all key bridge components to the corresponding system-wide and governing fragility curves.

Table 4: North-West Leg of Tower T3

					Sa (FN & FP)	Rel. Drift		strain		MDR
Scenario	RSN	Ground Motion Name	M	R (km)	(g)	at top (ft)	at PI (ft)	steel	concrete	ratio at PI
20	149	1979 Coyote Lake	5.74	4.79	0.10	0.45	0.13	-0.00013	0.00098	0.0013
19	147	1979 Coyote Lake	5.74	8.47	0.10	0.47	0.14	-0.00017	0.00099	0.0014
18	569	1986 San Salvador	5.80	3.71	0.10	0.43	0.13	-0.00011	0.00097	0.0013
17	4078	2004 Parkfield-02 CA	6.00	22.45	0.05	0.33	0.1	0.00006	0.00091	0.0010
13	8123	2011 Christchurch New Zealand	6.20	5.11	0.20	0.79	0.24	-0.00071	0.00116	0.0023
16	8099	2011 Christchurch New Zealand	6.20	17.86	0.10	0.4	0.12	-0.00006	0.00095	0.0012
22	159	1979 Imperial Valley-06	6.53	0.00	0.40	1.19	0.36	-0.00144	0.00134	0.0035
8	161	1979 Imperial Valley-06	6.53	8.54	0.38	0.73	0.22	-0.00059	0.00115	0.0021
15	313a	1981 Corinth Greece	6.60	10.27	0.10	0.49	0.15	-0.00021	0.00100	0.0015
26	313b	1981 Corinth Greece	6.60	10.27	0.10	0.55	0.16	-0.00030	0.00104	0.0016
14	1045b	1994 Northridge-01	6.69	2.11	0.20	0.55	0.16	-0.00030	0.00104	0.0016
6	1045a	1994 Northridge-01	6.69	2.11	0.35	0.72	0.22	-0.00059	0.00113	0.0021
23	1054	1994 Northridge-01	6.69	5.54	0.35	1.31	0.39	-0.00166	0.00139	0.0038
9	4847	2007 Chuetsu-oki Japan	6.80	9.43	0.23	0.9	0.27	-0.00091	0.00121	0.0026
21	1120	1995 Kobe Japan	6.90	1.46	0.48	1.48	0.44	-0.00229	0.00150	0.0043
7	1114	1995 Kobe Japan	6.90	3.31	0.32	1.14	0.34	-0.00135	0.00132	0.0033
12	292b	1980 Irpinia Italy-01	6.90	6.78	0.20	0.63	0.19	-0.00041	0.00111	0.0018
2	292a	1980 Irpinia Italy-01	6.90	6.78	0.40	0.95	0.28	-0.00100	0.00124	0.0027
10	6961	2010 Darfield New Zealand	7.00	13.37	0.12	0.62	0.19	-0.00043	0.00108	0.0018
11	6923	2010 Darfield New Zealand	7.00	30.53	0.12	0.5	0.15	-0.00021	0.00101	0.0015
5	5831	2010 El Mayor-Cucapah Mexico	7.20	14.80	0.18	0.76	0.23	-0.00066	0.00115	0.0022
4	864	1992 Landers	7.28	11.03	0.33	1.08	0.32	-0.00123	0.00129	0.0031
1	1176	1999 Kocaeli Turkey	7.51	1.38	0.48	1.31	0.39	-0.00166	0.00139	0.0038
3	1244	1999 Chi-Chi Taiwan	7.62	9.94	0.52	1.43	0.43	-0.00209	0.00146	0.0042
24	1236	1999 Chi-Chi Taiwan	7.62	37.48	0.20	0.81	0.24	-0.00075	0.00117	0.0023
25	2111	2002 Denali Alaska	7.90	42.99	0.10	0.38	0.11	-0.00003	0.00094	0.0011

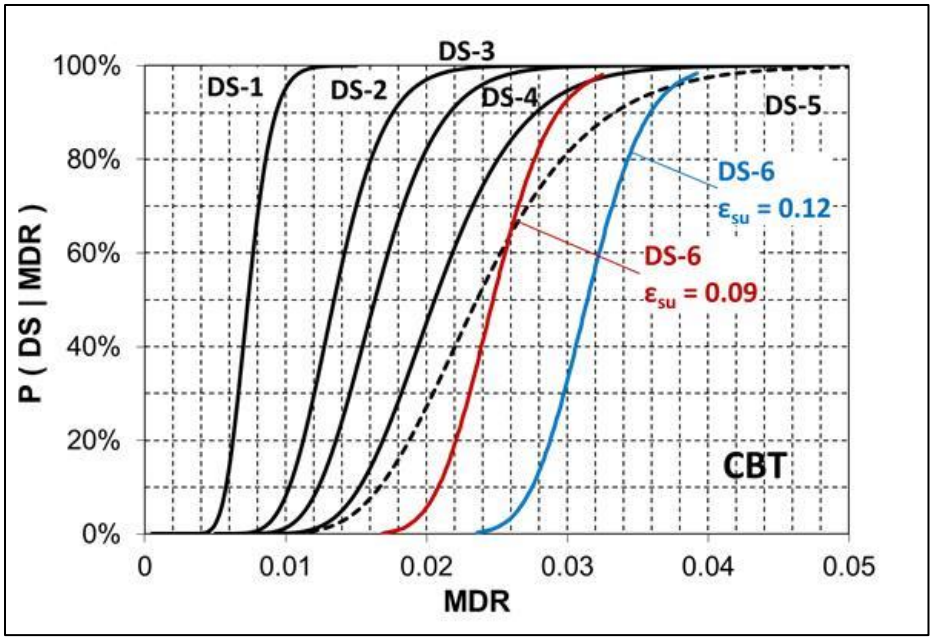

Figure 19: Maximum drift ratio fragility curves for T-3

References

1. Lilhanand, K. and Tseng W.S. (1987), "Generation of synthetic time histories compatible with multiple-damping response spectra.", Lausanne: SMiRT-9. K2/10.
2. Lilhanand, K. and Tseng W.S. (1988), "Development and application of realistic earthquake time histories compatible with multiple damping response spectra", Tokyo, Japan: Ninth World Conf. Earthquake Engineering, 1988. 819-824.
3. Somerville, P.G., N.F. Smith, R.W. Graves, and N.A. Abrahamson (1997). "Modification of empirical strong ground motion attenuation relations to include the amplitude and duration effects of rupture directivity", Seismological Research Letters 68, 199-222.
4. Mander et al. (1988), "Theoretical Stress-Strain Model for Confined Concrete", J. B. Mander; M. J. N. Priestley; and R. Park, Fellow, Journal of Structural Engineering, ASCE, Volume 14, Issue 8, September 1988.
5. American Society of Civil Engineers (1998). "Seismic Analysis of Safety-Related Nuclear Structures and Commentary." Reston, VA: ASCE, 4-98. 978-0-7844-0433-1.
6. Design Criteria (1999), Third Carquinez Strait Bridge Structural Design Criteria, Revision 6, 1 March, 1999, Prepared for the State of California, Department of Transportation, Division of Structures, Sacrament, California, by De Leuw, OPAC, Steinman, under contract 59A007.
7. Sedarat (1999), SC-Cable, Suspension Bridge Construction Sequence Application, Hassan Sedarat, SC Solutions, Inc., Sunnyvale, CA.

8. De Leuw–OPAC–Steinman (DLOS) (1999), "3rd Carquinez Strait Bridge Seismic Report", 100% submittal, Report, Submitted by: De Leuw – OPAC –Steinman, Caltrans Contract No. 59A0007, February, 1999.
9. Abrahamson, N.A. (2000) "Effects of rupture directivity on probabilistic seismic hazard analysis", Proceedings of the Sixth International Conference on Seismic Zonation, Earthquake Engineering Research Inst., Oakland, California.
10. DWG (2002), Construction Marked up Drawings of Alfred Zampa Memorial Bridge the Drawings.
11. Sleeter B.B., Calzia J.P., Walter S. R., Wong, F.L., and Saucedo G. J., (2004), "Earthquakes and faults in the San Francisco Bay Area (1970-2003)" http://pubs.usgs.gov/sim/2004/2848/, Last access, 085/27/2015.
12. ASCE 43-05 (2005), American Society of Civil Engineers (2005). "Seismic Design Criteria for Structures, Systems, and Components in Nuclear Facilities": American Society of Civil Engineers, 2005. ASCE/SEI 43-05.
13. SCS-NIST (2008), "Cyber-Enabled Wireless Monitoring Systems for the Protection of Deteriorating National Infrastructure Systems" Project, sponsored by NIST as part of the NIST TIP 2008 program, Development of detailed Finite Element Model of the New Carquinez Bridge, SC Solutions, 2008.
14. Baker, J. W., and Jayaram, N. (2008) "Correlation of spectral acceleration values from NGA ground motion models." Earthquake Spectra, 24(1), 299-317.
15. Atik, L.A. and Abrahamson, N. (2009) "An Improved Method for Nonstationary Spectral Matching." Earthquake Spectra, Vol. 26, No. 3, pp 601-617.
16. Vosooghi, Ashkan and Saiidi, M. Saiid (2010), "Seismic Damage States and Response Parameters for Bridge Columns" ACI Special Publication Series SP-271, Structural Concrete in Performance -Based Seismic Design of Bridges, 271 CD, 2010.
17. Baker, J. W. (2011), "Conditional Mean Spectrum: Tool for ground motion selection." Journal of Structural Engineering, 137(3), 322-331. http://dx.doi.org/10.1061/(ASCE)ST.1943-541X.0000215.
18. Gülerce, Z. and Abrahamson, N.A. (2011), "Site-Specific Design Spectra for Vertical Ground Motion." Earthquake Spectra: November 2011, Vol. 27, No. 4, pp. 1023-1047.
19. Shahi, S.K. and Baker, J. W. (2011), "An Empirically Calibrated Framework for Including the Effects of Near-Fault Directivity in Probabilistic Seismic Hazard Analysis." Bulletin of the Seismological Society of America, Vol. 101, No. 2, pp. 742-755.
20. Vosooghi, Ashkan and Saiidi, M. Saiid (2012), "Experimental Fragility Curves for Seismic Response of Reinforces Concrete Bridge Columns" ACI Structural Journal, November/December, 2012 pp 825-834.
21. Kurata, M., Kim, J., Lynch, J. P., van der Linden, G. W., Sedarat, H., Thometz, E., Hipley, P., Sheng, L. H (2013). "Internet-enabled Wireless Structural Monitoring Systems: Development and Permanent Deployment at the New Carquinez Suspension Bridge," Journal of Structural Engineering, ASCE, 139(10): 1688-1702.

22. Sedarat et al (2013), "Efficient Techniques in Finite Element Analysis and Seismic Evaluation of Suspension Bridges", Hassan Sedarat, Alexander Kozak, Joyce Lee, Alex Krimotat, Vince Jacob, Steve Mitchell, 7NSC -- Seventh National Seismic Conference on Bridges & Highways, Oakland, CA, May 20-22, 2013.

23. EMI (2014), "Kinematic Soil Pile Interaction for New Carquinez Bridge." Technical Memorandum, March 24, 2014, Earth Mechanics, Inc., Fountain Valley, CA.

24. Abrahamson, Silva and Kamai (2014), "NGA-West 2 equations for predicting PGA, PGV, and 5%-Damped PSA for shallow crustal earthquakes," Earthquake Spectra, 30.

25. Boore, D.M., J.P. Stewart, E. Seyhan, and G.M. Atkinson (2014), "NGA-West 2 equations for predicting PGA, PGV, and 5%-Damped PSA for shallow crustal earthquakes," Earthquake Spectra, 30.

26. Campbell, K.W. and Y. Bozorgnia (2014), "NGA-West 2 equations for predicting PGA, PGV, and 5%-Damped PSA for shallow crustal earthquakes, " Earthquake Spectra, 30.

27. Chiou, B.S.-J. and R.R. Youngs (2014), "NGA-West 2 equations for predicting PGA, PGV, and 5%-Damped PSA for shallow crustal earthquakes," Earthquake Spectra, 30.

28. Ancheta, T.D., Robert B. Darragh, Jonathan P. Stewart, Emel Seyhan, Walter J. Silva, Brian S.-J. Chiou, Katie E. Wooddell, Robert W. Graves, Albert R. Kottke, David M. Boore, Tadahiro Kishida, and Jennifer L. Donahue (2014) "NGA-West2 Database," Earthquake Spectra: August 2014, Vol. 30, No. 3, pp. 989-1005.

29. ATB (2014), ADINA Toll Bridges Project, sponsored by California Department of Transportation, Caltrans, 2014.

30. SCS (2015), "Rapid Post-Earthquake Safety Evaluation of the New Carquinez Bridge Using Fragility Curves and Strong-Motion Data: Seismic Hazard Memorandum." March 18, 2015, SC Solutions, Inc., Sunnyvale CA.

31. ADINA (2016), Automatic Dynamic Incremental Nonlinear Analysis, ADINA, ADINA R&D, 71 Elton Avenue, Watertown, MA 02472, USA.

32. SCMC (2016), an in-house section analysis program developed, SC Solutions, Inc., Sunnyvale, CA.

33. ATC-58 (2009), "Guidelines for Seismic Performance Assessment of Buildings," Applied Technology Council, Washington, D.C.

34. Massey, F. J. (1951). "The Kolmogorov-Smirnov Test for Goodness of Fit," Journal of the American Statistical Association, V. 46, No. 253, March, pp. 68-78.

35. Priestley, M. J. N.; Calvi, G. M.; and Kowalsky, M. J., (2007), Displacement-Based Seismic Design of Structures, IUSS Press, Pavia, Italy, 721 pp.

36. Caltrans (2013). "Seismic Design Criteria (SDC)," version 1.4, Calif. Dept. of Transportation, Sacramento, CA.